THE JOURNAL OF PHYSICAL CHEMISTRY C

Article

pubs.acs.org/JPCC

Surface Interrogation Scanning Electrochemical Microscopy (SI-SECM) of Photoelectrochemistry at a W/Mo-$BiVO_4$ Semiconductor Electrode: Quantification of Hydroxyl Radicals during Water Oxidation

Hyun S. Park, Kevin C. Leonard, and Allen J. Bard*

Center for Electrochemistry, Department of Chemistry and Biochemistry, The University of Texas at Austin, Austin, Texas 78712, United States

Supporting Information

ABSTRACT: Reaction kinetics and surface coverage of water oxidation intermediates at a W/Mo-$BiVO_4$ photoanode were studied using surface interrogation scanning electrochemical microscopy (SI-SECM). Adsorbed hydroxyl radicals (OH•) were produced during water oxidation at the semiconductor surface under UV−visible irradiation and were subsequently electrochemically titrated by tip-generated reductant without irradiation. The $IrCl_6^{2-/3-}$ redox couple was used to determine the surface concentration of OH• in acidic solution. On W/Mo-$BiVO_4$, ∼6% of the absorbed photons generate surface OH• with a coverage of 5.8 mC cm^{-2}. Less than 1% of the irradiated photons were eventually used for water oxidation under high intensity irradiation (∼1 W cm^{-2}) at the photoanode. Assuming that the primary decay mechanism of the adsorbed OH• on W/Mo-$BiVO_4$ is dimerization to produce hydrogen peroxide (H_2O_2), the rate constant was determined to be 4×10^3 mol^{-1} m^2 s^{-1}. A faster decay rate of OH• was observed in the presence of excess methanol (a radical scavenger) in aqueous solution. In addition, quantitative analysis of the water oxidation processes at W/Mo-$BiVO_4$ along with the quantum efficiency for the oxygen evolution reaction was determined using SECM.

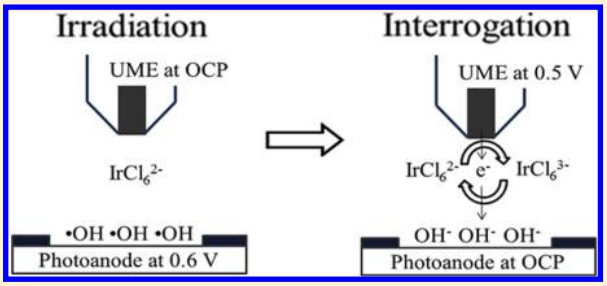

INTRODUCTION

The oxygen evolution reaction (OER) in aqueous solution has been extensively studied at photo- or electrocatalysts.[1−5] The intermediate radicals produced during water oxidation, for example, OH•, O•, or $H_2O^{\bullet+}$, have been detected, mostly at TiO_2 surfaces, using spin trapping, electron spin resonance (ESR) spectroscopy, fluorescence spectra, and infrared spectroscopy.[6−8] For example, the photogenerated OH• radicals at a Pt/TiO_2 surface were reported by the photocatalytic generation of salicylic acid from benzoic acid in an acidic aqueous solution.[9] Other kinds of surface radicals, for example, oxygen radical (O•) at a TiO_2 powder surface, have also been investigated using multiple internal reflection infrared spectroscopy (MIR-IR)[10] and ESR[11] during the OER under irradiation.

In photochemistry, the external quantum efficiency (EQE) (i.e., the ratio between the reaction products formed and the number of incident photons) and the internal quantum efficiency (IQE) (i.e., the ratio between the reaction products and the number of absorbed photons) are important figures to quantify the photoactivity and to analyze reaction mechanisms at the photocatalyst.[12,13] The quantum efficiency is a function of many different factors including illumination intensity, properties of the adsorbed species, the intrinsic properties of the semiconductor catalyst (e.g., electron/hole mobility, carrier lifetime, and doping density), and the reaction mechanisms of the redox couple in the solution.[14,15] For example, the EQE of the OH• formation at TiO_2 powder is <0.5%, as reported using spin trapping and ESR measurements.[16] Also, an IQE of ∼30% was obtained under very low-intensity irradiation (∼40 nW cm^{-2}) for organic compound decomposition through the formation of OH• at a TiO_2 film.[17] Recently, Zigah et al. reported the coverage of adsorbed OH• on TiO_2 nanotubes using the surface-interrogation mode of SECM (SI-SECM), but the quantum efficiencies were not calculated because the radiation intensity and absorbed number of photons at the electrode could not be measured due to the method of irradiation.[18] However, the amount of adsorbed OH• was reported to be 338 μC cm^{-2} for this nanostructured TiO_2.

Since its development in the late 1980s, SECM has proven to be a powerful tool for performing high-resolution chemical characterizations on all types of surfaces (insulating, semiconducting, and conducting) in solutions.[19,20] One area where SECM has been widely used is in studying mechanisms of heterogeneous inner-sphere reactions on catalytic surfaces. For example, the oxygen/hydrogen evolution reactions (OERs and

Received: January 15, 2013
Revised: May 15, 2013
Published: May 15, 2013

   dx.doi.org/10.1021/jp400478z | J. Phys. Chem. C 2013, 117, 12093−12102

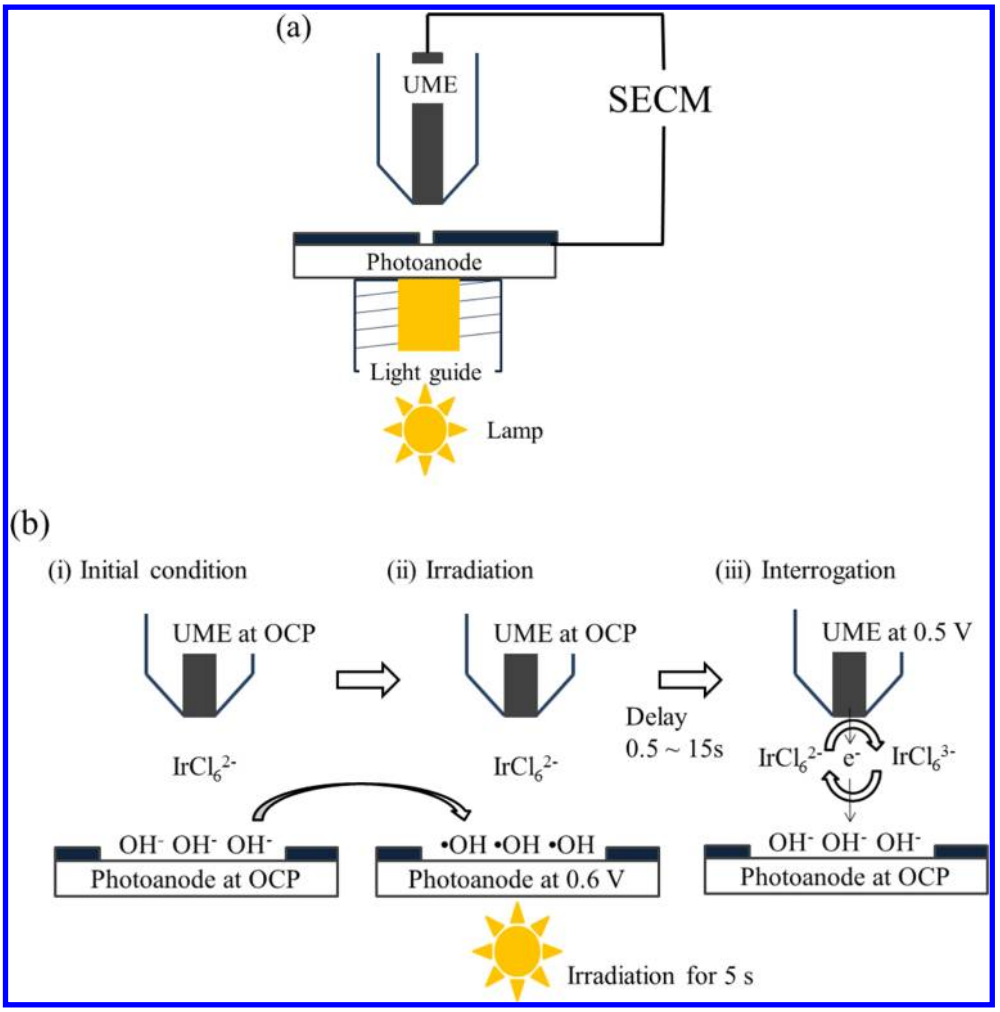

Figure 1. Schematic diagram of the experimental configurations of surface interrogation mode of SECM (a) and chemical reactions (b). The Au UME tip and W/Mo-$BiVO_4$ photoanode were allowed to rest at open circuit in the dark under initial conditions (b-i), then photon-injected to generate hydroxyl radicals (OH•) at W/Mo-$BiVO_4$ (b-ii), followed by the titrated using $IrCl_6^{2-/3-}$ couple in the dark (b-iii).

HERs), oxygen reduction reactions (ORRs), and hydrogen oxidation reactions (HORs) at Pt, Pd, Au, Hg, and other electrodes or nanoparticles have all been characterized using SECM.[21−23] In addition, studying reactions at semiconducting electrodes is also possible using SECM. One example is the one-electron outer-sphere oxidation kinetics of $Ru(NH_3)_6^{2+}$, which was investigated using the feedback mode of SECM at WSe_2 and Si electrodes without photon injection to the semiconductor.[24] In addition, the modification, degradation, and photooxidation of semiconductors (e.g., etching of GaAs, GaP, or CdTe surface using Br^-/Br_2 redox couple or the photooxidation of Ta_3N_5) have also been studied using SECM.[25,26] Recently, SECM was also used to discover new electrocatalysts, photocatalysts, and photosensitizers by combinatorial rapid screening methods.[27−30]

To perform these electrochemical characterizations, several techniques (or modes) of SECM have been developed that utilize an ultramicroelectrode (UME) tip with proper redox mediators in solutions.[31−36] The most popular modes of SECM include positive/negative feedback, tip generation/substrate collection (TG/SC), tip collection/substrate generation (TC/SG), and a redox competition mode of SECM.[37,38] Recently, SI-SECM has been introduced to study adsorbed surface species on an electrode; for example, a chemisorbed oxide layer on Au or Pt UME was titrated using $Ru(NH_3)_6^{2+/3+}$ and methyl viologen redox couples.[39,40] Also, SI-SECM was able to interrogate hydroxyl radicals (OH•) adsorbed on an illuminated nanostructured TiO_2 film.[18] In that study, the adsorbed radicals were generated from the oxidation of chemisorbed hydroxide ions by photogenerated holes at the nanostructured TiO_2 surface. With varying the time for the decay reaction of the radicals, for example, dimerization of OH• to hydrogen peroxide (H_2O_2), or its reaction with a radical scavenger (MeOH), a reversible $IrCl_6^{2-/3-}$ redox couple, was then used to titrate the remaining OH• at the surface using the transient feedback mode of SECM, that is, SI-SECM.

In this study, which builds on the SI-SECM mode demonstrated in the previous report,[18] we quantitatively study the water oxidation process at a W- and Mo-doped $BiVO_4$ (2 atomic % of W- and 6 atomic % of Mo-doped into $BiVO_4$, hereafter referred to as W/Mo-$BiVO_4$) electrode. $BiVO_4$ has been shown to be a promising n-type photocatalyst ever since Kudo et al. reported its photocatalytic activity in 1999.[41] In addition, W and Mo have been found to be effective shallow donors of $BiVO_4$ and increase the photocatalytic activity for both water oxidation and organic degradation.[42−46] SECM was also used to find an optimal ratio of W/Mo-$BiVO_4$

dx.doi.org/10.1021/jp400478z | J. Phys. Chem. C 2013, 117, 12093−12102

by rapid combinatorial screening for photocatalytic water oxidation.[42,47]

As described above, most of the surface studies on photocatalysts have been performed on various TiO_2 systems, and to the best of our knowledge no studies have yet been reported for $BiVO_4$. Herein, we report the SI-SECM of the adsorbed radicals at W/Mo-$BiVO_4$ electrodes and provide quantitative figures for the water oxidation reactions. Consequently, the results show the analytic scheme of photon absorption and water oxidation processes at W/Mo-$BiVO_4$ and the steps where efficiency losses occur.

EXPERIMENTAL SECTION

Chemicals. $Bi(NO_3)_3 \bullet 5H_2O$ (99.999%) and $(NH_4)_{10}H_2(W_2O_7)_6 \bullet xH_2O$ (99.99%) were purchased from Strem Chemicals (Newburyport, MA). VCl_3 (99%) and K_2IrCl_6 (99.95%) were purchased from Alfa-Aesar (Ward Hill, MA). $(NH_4)_6Mo_7O_{24} \bullet 4H_2O$ (99.98%), Na_2SO_4 (99.0%), Na_2SO_3 (99.6%), ferrocenemethanol (FcMeOH, 97%), and PbO_2 (97%) were obtained from Sigma-Aldrich (St. Louis, MO). NaH_2PO_4 (99.5%), Na_2HPO_4 (99.9%), and MeOH (99.9%) were purchased from Fisher Scientific (Pittsburgh, PA). Deionized Milli-Q water (D.I. water, 18 MΩ-cm) was used as the solvent for electrochemical experiments.

Electrodes. Fluorine-doped tin oxide (FTO, TEC 15, Pilkington, Toledo, OH) was used as a photoanode substrate. The UME tip electrode consisted of a Au wire (99.99%, Goodfellow, Devon, PA) with a diameter of 50 μm coated by a borosilicate glass sheath. The tip was polished using alumina suspensions (0.3 and 0.05 μm diameter powder, Buehler, Lake Bluff, IL) on abrasive disks (Figure S1a,b in the Supporting Information). W/Mo-$BiVO_4$ photoelectrodes were drop-cast onto the FTO substrate. In brief, 2.2 mM $Bi(NO_3)_3 \bullet 5H_2O$, 2.5 mM VCl_3, 8 μM $(NH_4)_{10}H_2(W_2O_7)_6 \bullet xH_2O$, and 43 μM $(NH_4)_6Mo_7O_{24} \bullet 4H_2O$ solutions in ethylene glycol were prepared. Then, 100 μL of the precursor solution was drop-cast on the FTO substrate (1.5 × 1.5 cm^2) and was annealed at 500 °C for 3h. Finally, expandable PTFE tape (maximum thickness of 88 μm, Fisher Scientific) was perforated using a needle (Easy touch, 31 gauge, 260 μm diameter), and the W/Mo-$BiVO_4$ electrode was covered by the perforated PTFE tape (Figure S1c,d in the Supporting Information). The depth and area of the exposed photoanode through the PTFE were measured using a Wyko NT9100 optical surface profiler (Veeco, New York). To ensure that solution was not leaking under the Teflon tape and contributing to the current response, the current density found for the exposed $BiVO_4$ spot was compared with that of a macroelectrode, and they were found to be identical. A Pt wire counter electrode and a saturated KCl Ag/AgCl reference electrode were used to complete the three-electrode configuration. However, all potentials reported here are quoted versus the normal hydrogen electrode (NHE).

Instruments. A scanning electrochemical microscope (SECM, model 920C, CH Instruments, Austin, TX) was used as for the electrochemical experiments. For the SECM experiments, an ELH bulb (300 W, GE 38476, General Electric, Fairfield, CT), with an emission intensity of ~900 mW/cm^2 over a wavelength region of 350 nm to longer than 1400 nm, was used as the light source in a custom-built enclosure with a cooling fan. A custom-made Teflon electrochemical cell was used to hold the three electrodes and a light guide (3 mm diameter) underneath the photoelectrode. Schematic presentations of the experimental configuration are shown in Figure 1. A silicon photodetector (model 818-UV) with an attenuator (OD3) and an optical power meter (model 1830-C) (Newport, Irvine, CA) were used to measure the irradiation intensities. A xenon lamp (XBO 150 W, Osram, Munich, Germany) with full output was also used to provide UV−visible irradiation.

Tip−Substrate Alignment. The exposed area of the W/Mo-$BiVO_4$ electrode and the thickness of the insulating layer around the W/Mo-$BiVO_4$ were measured before performing any electrochemical experiments to suitably place the tip UME above the photoanode and to quantify the results of the surface interrogation. Optical microscope images of the Au UME and the photoanode are shown in Figure S1 in the Supporting Information. Also shown is an optical surface profile, which was used to measure the exposed area of the photoanode, that is, 3.9×10^{-4} cm^2, where the Teflon insulator covered most of the substrate (Figure S1d in the Supporting Information). The thickness of the Teflon insulating tape around the exposed photoanode was ~20 μm.

Before performing the surface interrogation, the Au UME and the photoanode were aligned by measuring approach curves in a 1 mM FcMeOH, 0.1 M KCl aqueous solution. Cyclic voltammograms (CVs) of the Au UME in 1 mM FcMeOH showed typical steady-state behavior with the 50 μm UME (Figure S2a, Supporting Information). The diffusion-limited oxidation current of FcMeOH was measured at +0.7 V (vs NHE) at the Au UME, i_{Tip}, while the tip approached the insulating substrate at 5 μm s^{-1} using the stepper motor of the SECM (Figure S2b in the Supporting Information, approach curve of SECM). Because the flux of FcMeOH at the Au UME is limited by the very small tip−substrate distance, d, the oxidation current at the tip decreased, as shown in Figure S2b in the Supporting Information.[48] The approach curves were obtained at four different spots around the exposed W/Mo-$BiVO_4$ spot, while the vertical level of the substrate was aligned on the adjustable SECM stage. Finally, the Au UME tip was placed close to the substrate with d about 12 μm at $i_{Tip}/i_{infinite}$ = 0.4, where $i_{infinite}$ is the tip current measured far from the substrate.

After horizontally aligning the tip to the substrate, TC/SG-SECM was used to vertically place the UME above the exposed photoanode. To perform the TC/SG-SECM, the Au UME was placed at ~12 μm above the photoanode as discussed above. Then, the potential of the Au UME was set at 0.3 V for $FcMeOH^+$ reduction (TC), and the potential of the W/Mo-$BiVO_4$ electrode was held at 0.4 V under the light irradiation to oxidize the FcMeOH (SG). Figure S2c in the Supporting Information shows the scanning image obtained from TC/SG-SECM. The electrochemical image from SECM agrees well with the optical microscope image and the optical profile image, as shown in Figure S1c,d in the Supporting Information. Then, the Au UME was placed at the center of the W/Mo-$BiVO_4$ electrode, as determined from the scanning image of TC/SG-SECM. The tip was moved down an additional 20 μm to compensate for the Teflon thickness. At this point, the Au UME and W/Mo-$BiVO_4$ were properly aligned to perform the surface interrogation.

Before performing the surface interrogation experiment with $IrCl_6^{2-/3-}$, the collection efficiency, that is, the ratio of the tip current and the substrate current, of the $FcMeOH^{+/0}$ redox couple was measured for each electrode configuration. The current density for $FcMeOH^+$ reduction at the Au UME was 0.22 mA cm^{-2} and the photocurrent density for FcMeOH

dx.doi.org/10.1021/jp400478z | J. Phys. Chem. C 2013, 117, 12093−12102

oxidation was 0.38 mA cm^{-2} at W/Mo-$BiVO_4$ under irradiation at t = 30 s (Figure 2b), yielding a collection efficiency of 57%.

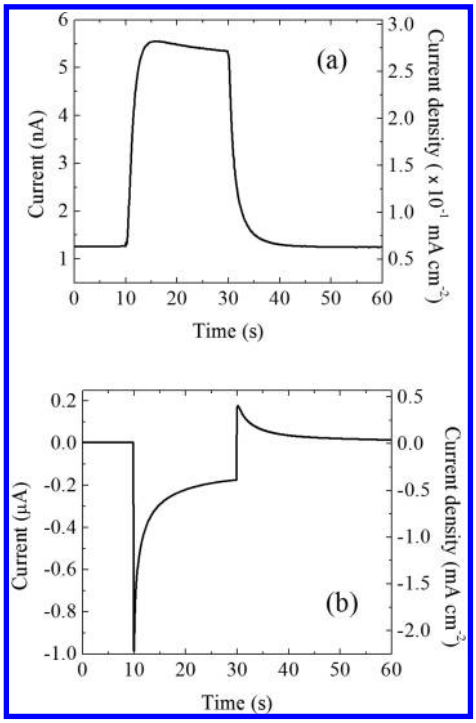

Figure 2. Tip collection current at Au UME (a) and substrate generation current at W/Mo-$BiVO_4$ (b) in a 1 mM FcMeOH and 0.1 M KCl aqueous solution. UV–visible irradiation was done from 10 to 30 s in the electrode configuration shown in Figure 1a. The potential of Au UME was 0.3 V (vs NHE) and W/Mo-$BiVO_4$ was held at 0.4 V. Au UME was placed ~12 μm above the substrate. The electrode area of the Au UME and the W/Mo-$BiVO_4$ electrode was 2.0×10^{-5} and 4.6×10^{-4} cm^2, respectively.

RESULTS AND DISCUSSION

Surface Interrogation. After the Au UME and the W/Mo-$BiVO_4$ electrodes were positioned at 12 μm apart as described above, the solution was changed to a 1 mM K_2IrCl_6 and 0.1 M Na_2SO_4 solution (pH 4.5) to perform the surface interrogation. Figure 1b shows a schematic of the experimental configurations with the corresponding chemical reactions for the SI-SECM used for these measurements. The $IrCl_6^{2-/3-}$ redox couple was used as the titrant because it has several favorable properties. First, the $IrCl_6^{2-/3-}$ redox couple has a fast reversible one-electron transfer reaction, and thus the rates of heterogeneous electron transfer for oxidation and reduction are high. Second, it is stable in the chemical environments used in these experiments and does not react with O_2 (the byproduct at the photoanode). Finally, there are no side reactions at the tip electrode, for example, O_2 reduction, at the potential used for the interrogation (tip potential of 0.5 V, Figure S3 in the Supporting Information).

A CV at the Au UME in the bulk solution away from the substrate shows a reduction current of $IrCl_6^{2-}$ (reaction 1, Figure 3):

$$IrCl_6^{2-} + e \leftrightarrow IrCl_6^{3-} \ (E^0 = 0.87 \text{ V vs NHE}) \quad (1)$$

For SI-SECM, OH• radicals were generated by the photogenerated holes at W/Mo-$BiVO_4$ under irradiation.

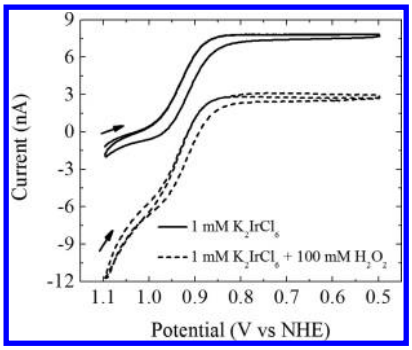

Figure 3. Cyclic voltammogram at Au UME tip in 1 mM K_2IrCl_6 and 0.1 M Na_2SO_4 aqueous solution (solid line) and in the presence of 0.1 M H_2O_2 (dashed line). Scan rate was 20 mV s^{-1}.

$$W/Mo\text{-}BiVO_4 + h\nu \rightarrow e^- + h^+ \quad (2)$$

$$OH^- + h^+ \rightarrow OH\bullet \ (E^0 = 1.8 \text{ V vs NHE, at pH 4.5}) \quad (3)$$

Stable adsorbed OH^- have been previously studied using infrared spectroscopy at a photoanode, for example, anatase TiO_2,[49,50] and the surface OH• produced from reaction 3 is the primary intermediate for photooxidation reactions in aqueous solutions at a TiO_2 surface.[16,51] For $BiVO_4$, nondissociative adsorption of water molecules at a Bi-site of $BiVO_4$ has been suggested from first-principle calculations.[52] However, no experimental observations of surface-adsorbed ions or water molecules in aqueous solutions at a $BiVO_4$ electrode have been previously reported. Here we assume that OH• is the dominant intermediate of water oxidation from the photogenerated holes, but the nature of its surface reactions still needs to be examined.

To interrogate the surface, we electrochemically produced $IrCl_6^{3-}$ at the Au UME, reaction 1 at a tip potential of 0.5 V. The $IrCl_6^{3-}$ diffused to the substrate in a few milliseconds and titrated the OH• at W/Mo-$BiVO_4$.

$$IrCl_6^{3-} + OH\bullet \rightarrow IrCl_6^{2-} + OH^- \quad (4)$$

The chemically produced $IrCl_6^{2-}$ diffused back to the tip; this positive feedback caused an increase in the reduction current for reaction 1 as long as OH• was present at the surface. When all of the OH• is consumed, the tip current decreases to the steady-state (negative feedback) value. For example, Figure 4a shows the chronoamperograms (CAs) of $IrCl_6^{2-}$ reduction at a Au UME with/without the adsorbed OH• on W/Mo-$BiVO_4$; the yellow line is the CA in the presence of the generated adsorbates after irradiation, and the gray line is without the adsorbed OH• (dark negative feedback current). The current difference between the two CAs indicates the amount of adsorbed radicals at the photoanode. However, if more time is allowed between the radical generation and the interrogation ("Delay" in Figure 1b), then the decay of the surface OH• occurs by (a) H_2O_2 generation from the dimerization of OH•, (b) desorption of the surface OH• to the bulk solution, and (c) surface reduction of the OH• back to OH^- by trapped electrons and solution reductants.

$$2OH\bullet \rightarrow H_2O_2 \ (\text{rate constant, } k) \quad (5)$$

$$OH\bullet(\text{adsorbed}) \rightarrow OH\bullet(\text{solution}) \quad (6)$$

$$OH\bullet(\text{adsorbed}) + e^- \rightarrow OH^- \quad (7)$$

Small amounts of H_2O_2 can be produced at W/Mo-$BiVO_4$ during the OH• generation. However, if there is excess H_2O_2 in

dx.doi.org/10.1021/jp400478z | J. Phys. Chem. C 2013, 117, 12093–12102

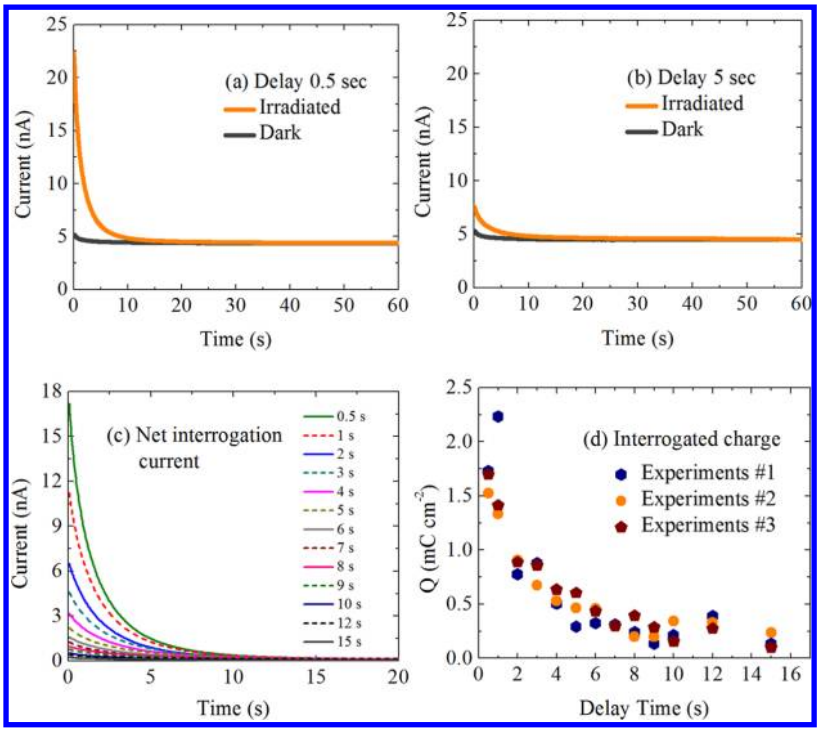

Figure 4. CAs of surface interrogation using Au UME on the W/Mo-$BiVO_4$ electrode with different decay times of (a) 0.5 and (b) 5 s after UV–visible irradiation for 5 s (yellow). CA of that without the irradiation is shown as a gray solid line in panels a and b. From the CAs, the net interrogation current, that is, current difference of CAs with/without the irradiation, was calculated in panel c with various decay times from 0.5 to 15 s. Then, the charge densities from repeated interrogation measurements were calculated in panel d. The potential of the Au UME was 0.5 V (vs NHE), and the W/Mo-$BiVO_4$ was held at 0.6 V during the irradiation. The potential and experimental configurations for the measurements were set as shown in Figure 1. Measurements were done in 1 mM K_2IrCl_6 and 0.1 M Na_2SO_4 aqueous solution. Au UME was placed about 12 μm above W/Mo-$BiVO_4$.

the solution, then it may decrease the interrogation current at the tip by chemical reaction 8 competing with electrochemical reduction reaction 1 at the tip.

$$H_2O_2 + 2IrCl_6^{2-} \rightarrow 2H^+ + O_2 + 2IrCl_6^{3-} \quad (8)$$

CV in the presence of excess H_2O_2 (100 mM) in the solution causes an increase in the current because of the EC reaction sequence involving reaction 8, as shown in Figure 3 (dotted line). Also, if desorbed OH• exists between the tip and the photoanode, then the interrogation current overestimates the amount of adsorbed OH• because reaction 4 can occur in solution. However, homogeneous reaction 8 is slow in contrast with the fast oxidation of $IrCl_6^{3-}$ with the energetic OH• in reaction 4.[18] Moreover, the tip response in CV attributable to reaction 8 was observed only in the presence of a relatively high concentration of H_2O_2 (100 mM), while the largest possible amount of H_2O_2 generated at the W/Mo-$BiVO_4$ surface was only on the order of picomoles, so that the amount of desorbed OH• from the substrate into solution can be considered to be negligible compared with that of adsorbed OH• at the semiconductor substrate.[16,51] Here the degree of surface recombination was also minimized by applying a positive bias to W/Mo-$BiVO_4$, that is, 0.6 V versus NHE, which results in ~0.8 eV of band bending based on the flat band potential of W/Mo-$BiVO_4$;[42] this promotes facile removal of the excited-electrons from the electrode surface and minimizes electron-trapping there. Thus surface reactions 4 and 5 can be assumed to be the dominant processes for the generation and consumption of OH• so that the amount of adsorbed OH• at the photoanode and the kinetic constant of OH• dimerization can be obtained as shown below.

$$dC_{OH\bullet}/dt = -kC_{OH\bullet}^2 \quad (9)$$

$$dC_{OH\bullet}/C_{\bullet OH}^2 = -k\,dt \quad (10)$$

$$1/C_{OH\bullet} = kt + 1/C_0 \quad (11)$$

where k is the rate constant of dimerization reaction 5; t is the time allowed for the dimerization; $C_{OH\bullet}$ is the surface concentration of adsorbed OH• at the photoanode at t; and C_0 is the surface coverage of OH• at $t = 0$. Therefore, if $C_{OH\bullet}$ is measured with different decay times using SI-SECM, then k and C_0 can be obtained from the slope and y intercept of eq 11.

To measure $C_{OH\bullet}$, we carried out SI-SECM with various decay times from 0.5 to 15 s. Figure 4a shows CAs with two different decay times of 0.5 and 5 s. (Also see Figure S4 in the Supporting Information.) At a longer decay times, the net interrogated current, that is, the difference between CAs measured with/without the irradiation, decreased as expected because more adsorbate disappeared. The resulting net interrogation currents are summarized in Figure 4c. The values of $C_{OH\bullet}$ at different times were obtained by integrating the net interrogation current, as shown in Figure 4d for experimental times of CAs ranging from 0 to 20 s.

A reciprocal plot of $C_{OH\bullet}$ with different decay times, shown in Figure 5 (eq 11), allows the determination of the rate constant of OH• dimerization, which was obtained as 0.4 mC^{-1} cm^2 s^{-1} or 4 × 10^3 mol^{-1} m^2 s^{-1} from the slope with a y intercept of 3.3 mC cm^{-2}. When the collection efficiency of the TC/SG-SECM is considered, that is, 57% as calculated in

dx.doi.org/10.1021/jp400478z | J. Phys. Chem. C 2013, 117, 12093–12102

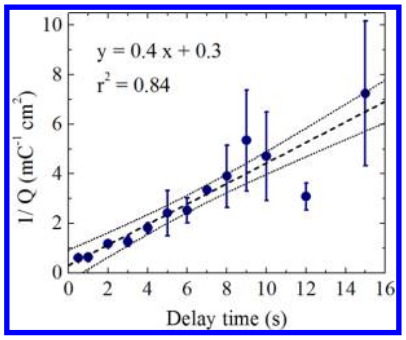

Figure 5. Reciprocal plot of the interrogation charges of OH• as a function of decay time. The interrogation charge was calculated as in Figure 4d from the repeated interrogation measurements. The trend line (dashed) and 95% confidence intervals (dotted) are drawn to show the slope and *y*-intercept deviations.

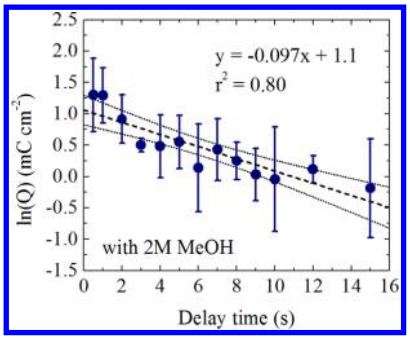

Figure 6. Plot of the interrogation charges of OH• as a function of decay time in the presence of excess MeOH in the solution. The trend line (dashed) and 95% confidence intervals (dotted) are drawn to show the slope and *y*-intercept deviations. SI-SECM was done in 1 mM K_2IrCl_6, 2 M MeOH, and 0.1 M Na_2SO_4 aqueous solution with the experimental details as in Figure 4.

Figure 2, the surface coverage of the adsorbed OH• was 5.8 mC cm^{-2} (or 60 nmol cm^{-2}, >1.7 mC cm^{-2} at 95% confidence level) at W/Mo-$BiVO_4$. The obtained coverage is about 20 times larger than that previously obtained from the nanotube TiO_2, that is, 338 μC cm^{-2}, under low-intensity irradiation by using SI-SECM.[18] Here the value obtained is within the range of that measured at TiO_2 thin films with adsorbed alcohols or dye.[17,53]

OH• Decay with Hole Scavenger. SI-SECM was further demonstrated to study the reaction of OH• with an electron donor, for example, MeOH.[54]

$$OH\bullet + CH_3OH \rightarrow H_2O + CH_2OH\bullet (\text{rate constant, } k_M) \quad (12)$$

As discussed above for the dimerization of OH•, the rate constant of reaction 12, k_M, and the surface coverage of OH• at W/Mo-$BiOV_4$ in the presence of a hole scavenger can be obtained using SI-SECM. Reaction 12 can be considered as a pseudo-first-order reaction with excess MeOH.[55−57] Then

$$dC_{OH\bullet}/dt = -k_M C_{OH\bullet} \quad (13)$$

$$dC_{OH\bullet}/C_{OH\bullet} = -k_M dt \quad (14)$$

$$\ln C_{OH\bullet} = -k_M t + \ln C_0 \quad (15)$$

SI-SECM was performed identically as shown above using a Au UME tip and a W/Mo-$BiVO_4$ substrate in 1 mM K_2IrCl_6, 2 M MeOH, and 0.1 M Na_2SO_4 aqueous solution. Figure 6 shows the results of the interrogation of OH• in the presence of excess MeOH. The apparent rate constant of reaction 12 was 0.1 s^{-1} obtained from the slope of eq 15, and the surface coverage of OH• was 5.1 mC cm^{-2} ($\pm$1.4 mC cm^{-2} at a 95% confidence interval) after correcting for the OH• dimerization and considering the collection efficiency of SI-SECM. As expected, the decay of OH• in the presence of the electron donor is fast and agrees with the previous report.[18] The obtained surface coverage of OH• also agreed well with that obtained without the scavenger as shown in Figure 5.

Estimated Photocurrent Efficiency. Surface coverage of the adsorbed OH• obtained from SI-SECM provides quantitative values for the reaction processes of water oxidation at the photoanode. Here the incident power through the light guide was ~980 mW cm^{-2}. Then, ~60 mW cm^{-2} was absorbed by the W/Mo-$BiVO_4$ film with a thickness of ~200 nm. If the average energy of absorbed photons is assumed to be 3 eV, taking into account the spectrum of the incident light and the band gap and absorbance of W/Mo-$BiVO_4$,[42] then the rate of photon absorption was ~1.2×10^{17} cm^{-2} s^{-1}.

$$\text{rate of absorbed photon} = 60 \text{ mJ cm}^{-2} \text{ s}^{-1}/(3 \text{ eV} \times 1.6 \times 10^{-19} \text{ J eV}^{-1}) = 1.2 \times 10^{17} \text{ cm}^{-2} \text{ s}^{-1} \quad (16)$$

The number of W/Mo-$BiVO_4$ molecules in the electrode was ~1.3×10^{17} cm^{-2} based on the density of $BiVO_4$ and properties of the film applied on the electrode, that is, 0.22 μmol cm^{-2} with a ~200 nm film thickness. Consequently, the excitation rate of W/Mo-$BiVO_4$ was ~1 s^{-1} $molecule^{-1}$ under the irradiation conditions used. Thus, only ~6% of the absorbed photons were used to produce the surface OH• of 5.8 mC cm^{-2} or 3.6×10^{16} cm^{-2}, as obtained above after 5 s of the irradiation.

$$\%OH\bullet \text{ to absorbed photon} = 3.6 \times 10^{16} \text{ cm}^{-2}/(1.2 \times 10^{17} \text{ cm}^{-2} \text{ s}^{-1} \times 5 \text{ s}) \times 100 = 6\% \quad (17)$$

The results from SI-SECM indicate that ~94% of the excited electron−hole pairs produced by the injected photons during the 5 s recombined either in the bulk or at the surface of W/Mo-$BiVO_4$.

As previously mentioned, the percent of generated holes that react with the chemisorbed OH^- at the electrode surface is a function of the total flux of photons absorbed in the photocatalysts.[14,16] In this work, the amount of surface OH• was also a function of the illumination time (Figure S5 in the Supporting Information), and the surface coverage showed asymptotic growth as the illumination time increased. The coverage of radicals may reach saturation with illumination times longer than 5 s at W/Mo-$BiVO_4$ under the irradiation intensity used here, but irradiation times longer than 5 s were not used so as to avoid bubble generation at the substrate. However, even with 1 s of irradiation, the interrogated charge was >50% of that obtained after 5 s of irradiation. The results indicate that >15% of the absorbed photons were initially used to produce the adsorbed radicals, and the efficiency decreased to 6% after 5 s of irradiation. In other words, the quantum efficiency of the absorbed photon conversion to the adsorbed OH• decreased asymptotically, as shown in Figure S5 in the Supporting Information.

The minority carrier flux, which reached the electrode surface without surface recombination, was estimated from a fast

dx.doi.org/10.1021/jp400478z | J. Phys. Chem. C 2013, 117, 12093−12102

irreversible reaction, for example, sulfite oxidation, at W/Mo-$BiVO_4$.[45] Figure S6 in the Supporting Information shows the photocurrent for sulfite oxidation at a large W/Mo-$BiVO_4$ electrode with a film thickness of 200 nm under various irradiation intensities. Although the light intensities used in Figure S6 in the Supporting Information were about half of that used for SI-SECM, that is, ~400 mW cm^{-2}, the sulfite oxidation current in Figure S6 in the Supporting Information approached the saturated values with increased irradiation intensity, and the excited-hole flux at the electrode surface was calculated from the photocurrent. The excited-hole flux at 0.6 V was:

$$\begin{aligned}&\text{hole flux at electrode surface} = 1.8 \times 10^{-3}\ \text{C s}^{-1}\ \text{cm}^{-2} \\ &/(96485\ \text{C mol}^{-1}) \times 6.02 \times 10^{23}\ \text{mol} \\ &= 1.1 \times 10^{16}\ \text{cm}^{-2}\ \text{s}^{-1} \end{aligned} \quad (18)$$

Thus, the hole-flux at the surface without surface recombination corresponded to ~9% of the absorbed photon flux, that is, 1.2×10^{17} cm^{-2} s^{-1}. This indicates that ~91% of excited electron−hole pairs recombined before they reached the surface.

The water oxidation current was also measured to calculate the quantum efficiency for the photon-conversion to oxygen evolution. Figure 7 shows the water oxidation current at W/Mo-$BiVO_4$ under chopped irradiation. The measured current for water oxidation was ~0.2 mA cm^{-2} at 0.6 V (pH 7), which corresponds to a hole flux of 1.2×10^{15} cm^{-2} s^{-1}, that is, 1% of the absorbed photons. The obtained IQE was smaller than the previously reported value, for example, 5−10%,[42] mainly because of the higher irradiation intensity used here. Moreover, the obtained current measured here was in a more basic solution (pH 7) than that used in SI-SECM (pH 4.5), and the water oxidation efficiency will be smaller in the more acidic medium. However, the obtained hole flux for water oxidation corresponded to 11% of the holes that reached the surface without surface recombination (1.1×10^{16} cm^{-2} s^{-1}). In other words, 89% of the hole flux at the electrode surface (9.8×10^{15} cm^{-2} s^{-1}) was consumed by surface recombination with electrons produced near the surface. The extent of surface recombination for 1 s corresponds to ~30% of the surface-adsorbed OH• (3.6×10^{16} cm^{-2}). If we assume that reaction 7 is the major process of the surface recombination, then ~30% of surface OH• was reduced and regenerated by excited electron−hole pairs for every second at steady state. The calculations are summarized in Figure 8 and Table 1.

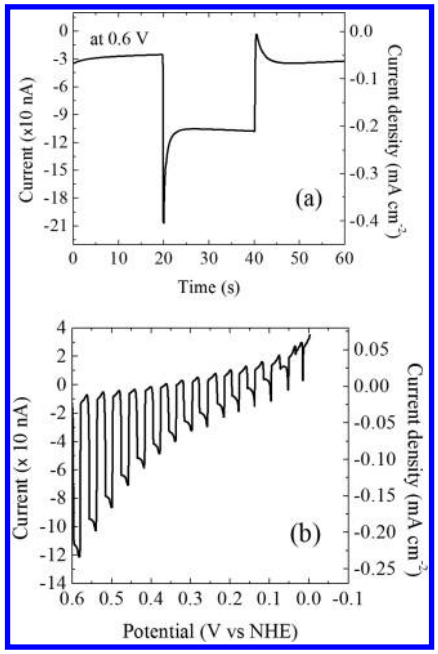

Figure 7. Chronoamperogram of photocurrent for water oxidation at W/Mo-$BiVO_4$ electrode at 0.6 V (vs NHE) (a) and its linear sweep voltammogram (b) in 0.1 M Na_2SO_4 aqueous solution (pH 7). UV−visible irradiation was switched on from 20 to 40 s in panel a. Scan rate was 20 mV s^{-1} in panel b. Electrode area was 5.1×10^{-4} cm^{-2} and the experimental conditions were as shown in Figure 1.

The quantitative analysis from SI-SECM measurements indicates that the most significant loss of photon energy conversion to chemical energy at W/Mo-$BiVO_4$ is from the bulk recombination, that is, 91% of the absorbed photons. The surface recombination loss is also significant, that is, ~8% of the absorbed photons or ~30% of the surface OH• underwent recombination every second. The recombination loss should be addressed to further increase the photoactivity of W/Mo-$BiVO_4$. It has been widely reported that surface recombination can largely be reduced by using electrocatalysts, for example, IrO_x, Co_3O_4, Pt, and cobalt oxide deposited from a phosphate medium (Co-Pi) for water oxidation.[45,58] Bulk recombination of $BiVO_4$ has been reduced by doping the W, Mo, or P[42,47,59] or fabricating a heterojunction, for example, WO_3 or SnO_2, to $BiVO_4$.[60−63] The quantum efficiency is also a function of the thickness of the semiconductor film that affects the photon absorption, carrier transport, and the bulk recombination.[64,65] Furthermore the illumination configuration, for example, electrode side (back) or solution side (front) illumination, can also affect the ratio between different recombination processes, for example, bulk or contact versus surface recombination. However, this study focused only on back illumination. In summary, many factors affect the performance of photoelectrodes including the electrode geometry, intrinsic properties of photocatalysts, illumination configuration, and the surface states on the electrodes. The techniques mentioned above will be investigated to improve the quantum efficiencies of W/Mo-$BiVO_4$, and SI-SECM will be used as a versatile tool to elucidate the effects of the modification of the photoelectrodes.

■ CONCLUSIONS

SI-SECM has been used to study the photogenerated surface OH• during water oxidation at W/Mo-$BiVO_4$. The OH• produced under strong irradiation at the W/Mo-$BiVO_4$ surface was interrogated using an $IrCl_6^{2-/3-}$ redox couple as the titrant of the radicals. The surface coverage of OH• obtained was 5.8 mC cm^{-2} after 5 s of UV−visible irradiation at W/Mo-$BiVO_4$. The kinetic rate constant of OH• dimerization to produce H_2O_2 was measured as 4×10^3 mol^{-1} m^2 s^{-1}. In a solution having excess hole scavenger, that is, 2 M MeOH, OH• experienced fast decay with a kinetic rate constant of 0.1 s^{-1}. Quantitative measurements showed that ~6% of the absorbed photons contribute to the production of adsorbed OH• at W/Mo-$BiVO_4$. However, >90% of the excited electron−hole pairs underwent bulk-recombination before reaching the electrode surface. About 30% of the adsorbed OH•, which corresponds to 8% of the absorbed photon flux, was reduced by surface recombination every second. Finally, only 1% of the absorbed photons were used for water oxidation at W/Mo-$BiVO_4$ under strong irradiation.

dx.doi.org/10.1021/jp400478z | J. Phys. Chem. C 2013, 117, 12093−12102

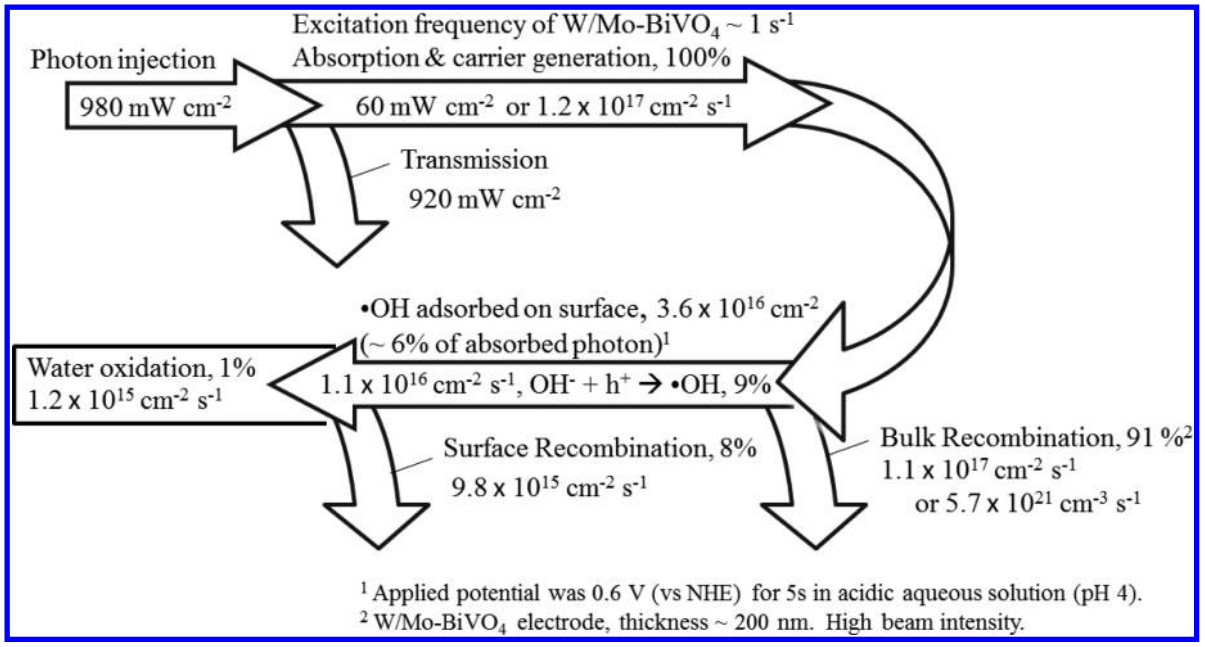

Figure 8. Schematic representations of the photon and minority carrier reaction processes of the W/Mo-$BiVO_4$ for water oxidation. Quantitative values were calculated from the results in Figures 5 and 7 and Supporting Information Figure S6 with the experimental conditions stated therein.

Table 1. Summary of SI-SECM Measurements[a]

		decay of OH•	
	surface coverage of OH• (mC cm^{-2})	reaction	rate constant
w/o scavenger	5.8	2•OH → H_2O_2	4×10^3 mol^{-1} m^2 s^{-1}
with 2 M MeOH	5.1	•OH + MeOH → product	0.1 s^{-1}

[a]Surface coverage and rate constant of radical reactions were obtained from Figures 5 and 6.

■ ASSOCIATED CONTENT

Ⓢ Supporting Information

Additional experimental details. This material is available free of charge via the Internet at http://pubs.acs.org.

■ AUTHOR INFORMATION

Corresponding Author

*E-mail: ajbard@mail.utexas.edu.

Notes

The authors declare no competing financial interest.

■ ACKNOWLEDGMENTS

This work was funded by the Samsung SAIT GRO Program, the Division of Chemical Sciences, Geosciences, and Biosciences Office of Basic Energy Sciences of the U.S. Department of Energy-SISGR (DE-FG02-09ER16119) and the Robert A. Welch Foundation (F-0021).

■ REFERENCES

(1) Barber, J. Photosynthetic Energy Conversion: Natural and Artificial. *Chem. Soc. Rev.* **2009**, *38*, 185−196.

(2) Nakamura, R.; Okamura, T.; Ohashi, N.; Imanishi, A.; Nakato, Y. Molecular Mechanisms of Photoinduced Oxygen Evolution, PL Emission, and Surface Roughening at Atomically Smooth (110) and (100) n-TiO_2 (Rutile) Surfaces in Aqueous Acidic Solutions. *J. Am. Chem. Soc.* **2005**, *127*, 12975−12983.

(3) Subbaraman, R.; Tripkovic, D.; Chang, K.-C.; Strmcnik, D.; Paulikas, A. P.; Hirunsit, P.; Chan, M.; Greeley, J.; Stamenkovic, V.; Markovic, N. M. Trends in Activity for the Water Electrolyser Reactions on 3d M(Ni,Co,Fe,Mn) Hydr(oxy)oxide catalysts. *Nat. Mater.* **2012**, *11*, 550−557.

(4) Zong, R.; Thummel, R. P. A New Family of Ru Complexes for Water Oxidation. *J. Am. Chem. Soc.* **2005**, *127*, 12802−12803.

(5) Clausen, J.; Junge, W. Detection of an Intermediate of Photosynthetic Water Oxidation. *Nature* **2004**, *430*, 480−483.

(6) Jaeger, C. D.; Bard, A. J. Spin Trapping and Electron Spin Resonance Detection of Radical Intermediates in the Photodecomposition of Water at Titanium Dioxide Particulate Systems. *J. Phys. Chem.* **1979**, *83*, 3146−3152.

(7) Ahmed, A. Y.; Kandiel, T. A.; Oekermann, T.; Bahnemann, D. Photocatalytic Activities of Different Well-Defined Single Crystal TiO_2 Surfaces: Anatase versus Rutile. *J. Phys. Chem. Lett.* **2011**, *2*, 2461−2465.

(8) Schwarz, P. F.; Turro, N. J.; Bossmann, S. H.; Braun, A. M.; Wahab, A.-M. A. A.; Durr, H. A New Method to Determine the Generation of Hydroxyl Radicals in Illuminated TiO_2 Suspensions. *J. Phys. Chem. B* **1997**, *101*, 7127−7134.

(9) Izumi, I.; Fan, F.-R. F.; Bard, A. J. Heterogeneous Photocatalytic Decomposition of Benzoic Acid and Adipic Acid on Platinized Titanium Dioxide Powder. The Photo-Kolbe Decarboxylative Route to the Breakdown of the Benzene Ring and to the Production of Butane. *J. Phys. Chem.* **1981**, *85*, 218−223.

(10) Nakamura, R.; Nakato, Y. Primary Intermediates of Oxygen Photoevolution Reaction on TiO_2 (Rutile) Particles, Revealed by in Situ FTIR Absorption and Photoluminescence Measurements. *J. Am. Chem. Soc.* **2004**, *126*, 1290−1298.

(11) Micic, O. I.; Zhang, Y.; Cromack, K. R.; Trifunac, A. D.; Thurnauer, M. C. Trapped Holes on Titania Colloids Studied by Electron Paramagnetic Resonance. *J. Phys. Chem.* **1993**, *97*, 7277−7283.

(12) Park, S. H.; Roy, A.; Beaupre, S.; Cho, S.; Coates, N.; Moon, J. S.; Moses, D.; Leclerc, M.; Lee, K.; Heeger, A. J. Bulk Heterojunction

Solar Cells With Internal Quantum Efficiency Approaching 100%. *Nat. Photon.* **2009**, *3*, 297−303.
(13) Nozik, A. J. Exciton Multiplication and Relaxation Dynamics in Quantum Dots: Applications to Ultrahigh-Efficiency Solar Photon Conversion. *Inorg. Chem.* **2005**, *44*, 6893−6899.
(14) Nosaka, Y.; Fox, M. A. Effect of Light Intensity on the Quantum Yield of Photoinduced Electron Transfer From Colloidal Cadmium Sulfide to Methylviologen. *J. Phys. Chem.* **1986**, *90*, 6521−6522.
(15) Ishibashi, K.; Fujishima, A.; Watanabe, T.; Hashimoto, K. Generation and Deactivation Processes of Superoxide Formed on TiO_2 Film Illuminated by Very Weak UV Light in Air or Water. *J. Phys. Chem. B* **2000**, *104*, 4934−4938.
(16) Nosaka, Y.; Komori, S.; Yawata, K.; Hirakawa, T.; Nosaka, A. Y. Photocatalytic •OH Radical Formation in TiO_2 Aqueous Suspension Studied by Several Detection Methods. *Phys. Chem. Chem. Phys.* **2003**, *5*, 4731−4735.
(17) Ohko, Y.; Hashimoto, K.; Fujishima, A. Kinetics of Photocatalytic Reactions Under Extremely Low-Intensity UV-Illumination on Titanium Dioxide Thin Films. *J. Phys. Chem. A* **1997**, *101*, 8057−8062.
(18) Zigah, D.; Rodriguez-Lopez, J.; Bard, A. J. Quantification of Photoelectrogenerated Hydroxyl Radical on TiO_2 by Surface Interrogation Scanning Electrochemical Microscopy. *Phys. Chem. Chem. Phys.* **2012**, *14*, 12764−12772.
(19) Bard, A. J.; Fan, F.-R. F.; Kwak, J.; Lev, O. Scanning Electrochemical Microscopy. Introduction and Principles. *Anal. Chem.* **1989**, *61*, 132−138.
(20) Kwak, J.; Bard, A. J. Scanning Electrochemical Microscopy. Theory of the Feedback Mode. *Anal. Chem.* **1989**, *61*, 1221−1227.
(21) Sanchez-Sanchez, C. M.; Rodriguez-Lopez, J.; Bard, A. J. Scanning Electrochemical Microscopy. 60. Quantitative Calibration of the SECM Substrate Generation/Tip Collection Mode and Its Use for the Study of the Oxygen Reduction Mechanism. *Anal. Chem.* **2008**, *80*, 3254−3260.
(22) Bertoncello, P. Advances on Scanning Electrochemical Microscopy (SECM) for Energy. *Energy Environ. Sci.* **2010**, *3*, 1620−1633.
(23) Shah, B. C.; Hillier, A. C. Imaging the Reactivity of Electrooxidation Catalysts With the Scanning Electrochemical Microscope. *J. Electrochem. Soc.* **2000**, *147*, 3043−3048.
(24) Horrocks, B. R.; Mirkin, M. V.; Bard, A. J. Scanning Electrochemical Microscopy. 25. Application to Investigation of the Kinetics of Heterogeneous Electron Transfer at Semiconductor (WSe_2 and Si) Electrodes. *J. Phys. Chem.* **1994**, *98*, 9106−9114.
(25) Mandler, D.; Bard, A. J. High Resolution Etching of Semiconductors by the Feedback Mode of the Scanning Electrochemical Microscope. *J. Electrochem. Soc.* **1990**, *137*, 2468−2472.
(26) Cong, Y.; Park, H. S.; Wang, S.; Dang, H. X.; Fan, F.-R. F.; Mullins, C. B.; Bard, A. J. Synthesis of Ta_3N_5 Nanotube Arrays Modified with Electrocatalysts for Photoelectrochemical Water Oxidation. *J. Phys. Chem. C* **2012**, *116*, 14541−14550.
(27) Fernandez, J. L.; Walsh, D. A.; Bard, A. J. Thermodynamic Guidelines for the Design of Bimetallic Catalysts for Oxygen Electroreduction and Rapid Screening by Scanning Electrochemical Microscopy. M-Co (M: Pd, Ag, Au). *J. Am. Chem. Soc.* **2005**, *127*, 357−365.
(28) Kylberg, W.; Wain, A. J.; Castro, F. A. Screening of Photoactive Dyes on TiO_2 Surfaces Using Scanning Electrochemical Microscopy. *J. Phys. Chem. C* **2012**, *116*, 17384−17392.
(29) Ye, H.; Park, H. S.; Bard, A. J. Screening of Electrocatalysts for Photoelectrochemical Water Oxidation on W-Doped $BiVO_4$ Photocatalysts by Scanning Electrochemical Microscopy. *J. Phys. Chem. C* **2011**, *115*, 12464−12470.
(30) Lee, J.; Ye, H.; Pan, S.; Bard, A. J. Screening of Photocatalysts by Scanning Electrochemical Microscopy. *Anal. Chem.* **2008**, *80*, 7445−7450.
(31) Mirkin, M. V.; Nogala, W.; Velmurugan, J.; Wang, Y. Scanning Electrochemical Microscopy in the 21st Century. Update 1: Five Years After. *Phys. Chem. Chem. Phys.* **2011**, *13*, 21196−21212.
(32) Zaera, F. Probing Liquid/Solid Interfaces at the Molecular Level. *Chem. Rev.* **2012**, *112*, 2920−2986.
(33) Snowden, M. E.; Guell, A. G.; Lai, S. C. S.; McKelvey, K.; Ebejer, N.; O'Connell, M. A.; Colburn, A. W.; Unwin, P. R. Scanning Electrochemical Cell Microscopy: Theory and Experiment for Quantitative High Resolution Spatially-Resolved Voltammetry and Simultaneous Ion-Conductance Measurements. *Anal. Chem.* **2012**, *84*, 2483−2491.
(34) Lee, C.; Kwak, J.; Bard, A. J. Application of Scanning Electrochemical Microscopy to Biological Samples. *Proc. Natl. Acad. Sci. U.S.A.* **1990**, *87*, 1740−1743.
(35) Patten, H. V.; Lai, S. C. S.; Macpherson, J. V.; Unwin, P. R. Active Site for Outer-Sphere, Inner-Sphere, and Complex Multistage Electrochemical Reactions at Polycrystalline Boron-Doped Diamond Electrodes (pBDD) Revealed with Scanning Electrochemical Cell Microscopy (SECCM). *Anal. Chem.* **2012**, *84*, 5427−5432.
(36) Grisotto, F.; Ghorbal, A.; Goyer, C.; Charlier, J.; Palacin, S. Direct SECM Localized Electrografting of Vinylic Monomers on a Conducting Substrate. *Chem. Mater.* **2011**, *23*, 1396−1405.
(37) Bard, A. J.; Mirkin, M. V.; Unwin, P. R.; Wipf, D. O. Scanning Electrochemical Microscopy. 12. Theory and Experiment of the Feedback Mode With Finite Heterogeneous Electron-Transfer Kinetics and Arbitrary Substrate Size. *J. Phys. Chem.* **1992**, *96*, 1861−1868.
(38) Eckhard, K.; Chen, X.; Turcu, F.; Schuhmann, W. Redox Competition Mode of Scanning Electrochemical Microscopy (RC-SECM) for Visualisation of Local Catalytic Activity. *Phys. Chem. Chem. Phys.* **2006**, *8*, 5359−5365.
(39) Rodriguez-Lopez, J.; Alpuche-Aviles, M. A.; Bard, A. J. Interrogation of Surfaces for the Quantification of Adsorbed Species on Electrodes: Oxygen on Gold and Platinum in Neutral Media. *J. Am. Chem. Soc.* **2008**, *130*, 16985−16995.
(40) Rodriguez-Lopez, J.; Minguzzi, A.; Bard, A. J. Reaction of Various Reductants with Oxide Films on Pt Electrodes as Studied by the Surface Interrogation Mode of Scanning Electrochemical Microscopy (SI-SECM): Possible Validity of a Marcus Relationship. *J. Phys. Chem. C* **2010**, *114*, 18645−18655.
(41) Kudo, A.; Omori, K.; Kato, H. A Novel Aqueous Process for Preparation of Crystal Form-Controlled and Highly Crystalline $BiVO_4$ Powder From Layered Vanadates at Room Temperature and Its Photocatalytic and Photophysical Properties. *J. Am. Chem. Soc.* **1999**, *121*, 11459−11467.
(42) Park, H. S.; Kweon, K. E.; Ye, H.; Paek, E.; Hwang, G. S.; Bard, A. J. Factors in the Metal Doping of $BiVO_4$ for Improved Photoelectrocatalytic Activity as Studied by Scanning Electrochemical Microscopy and First-Principles Density-Functional Calculation. *J. Phys. Chem. C* **2011**, *115*, 17870−17879.
(43) Berglund, S. P.; Rettie, A. J. E.; Hoang, S.; Mullins, C. B. Incorporation of Mo and W Into Nanostructured $BiVO_4$ for Efficient Photoelectrochemical Water Oxidation. *Phys. Chem. Chem. Phys.* **2012**, *14*, 7065−7075.
(44) Pilli, S. K.; Furtak, T. E.; Brown, L. D.; Deutsch, T. G.; Turner, J. A.; Herring, A. M. Cobalt-phosphate (Co-Pi) Catalyst Modified Mo-doped $BiVO_4$ Photoelectrodes for Solar Water Oxidation. *Energy Environ. Sci.* **2011**, *4*, 5028−5034.
(45) Zhong, D. K.; Choi, S.; Gamelin, D. R. Near-Complete Suppression of Surface Recombination in Solar Photoelectrolysis by "Co-Pi" Catalyst-Modified W:$BiVO_4$. *J. Am. Chem. Soc.* **2011**, *133*, 18370−18377.
(46) Kontic, R.; Patzke, G. R. Synthetic Trends for $BiVO_4$ Photocatalysts: Molybdenum Substitution vs. TiO_2 and SnO_2 Heterojunctions. *J. Solid State Chem.* **2012**, *189*, 38−48.
(47) Ye, H.; Lee, J.; Jang, J. S.; Bard, A. J. Rapid Screening of $BiVO_4$-based Photocatalysts by Scanning Electrochemical Microscopy (SECM) and Studies of Their Photoelectrochemical Properties. *J. Phys. Chem. C* **2010**, *114*, 13322−13328.
(48) Sun, P.; Laforge, F. O.; Mirkin, M. V. Scanning Electrochemical Microscopy in the 21st Century. *Phys. Chem. Chem. Phys.* **2007**, *9*, 802−823.

(49) Tanaka, K.; White, J. M. Characterization of Species Adsorbed on Oxidized and Reduced Anatase. *J. Phys. Chem.* **1982**, *86*, 4708−4714.
(50) Primet, M.; Pichat, P.; Mathieu, M.-V. Infrared Study of the Surface of Titanium Dioxides. I. Hydroxyl Groups. *J. Phys. Chem.* **1971**, *75*, 1216−1220.
(51) Lawless, D.; Serpone, N.; Meisel, D. Role of Hydroxyl Radicals and Trapped Holes in Photocatalysis. A Pulse Radiolysis Study. *J. Phys. Chem.* **1991**, *95*, 5166−5170.
(52) Ohikiri, M.; Boero, M. Water Molecule Adsorption Properties on the $BiVO_4$ (100) Surface. *J. Phys. Chem. B.* **2006**, *110*, 9188−9194.
(53) Shankar, K.; Basham, J. I.; Allam, N. K.; Varghese, O. K.; Mor, G. K.; Feng, X.; Paulose, M.; Seabold, J. A.; Choi, K.-S.; Grimes, C. A. Recent Advances in the Use of TiO_2 Nanotube and Nanowire Arrays for Oxidative Photoelectrochemistry. *J. Phys. Chem. C* **2009**, *113*, 6327−6359.
(54) Ulanski, P.; Von Sonntag, C. The OH Radical-induced Chain Reactions of Methanol With Hydrogen Peroxide and With Peroxodisulfate. *J. Chem. Soc., Perkin Trans. 2* **1999**, *2*, 165−168.
(55) Hess, W. P.; Tully, F. P. Hydrogen-Atom Abstraction From Methanol by Hydroxyl Radical. *J. Phys. Chem.* **1989**, *93*, 1944−1947.
(56) Jimenez, E.; Gilles, M. K.; Ravishankara, A. R. Kinetics of the Reactions of the Hydroxyl Radical With CH_3OH and C_2H_5OH Between 235 and 360 K. *J. Photochem. Photobiol. A-Chem.* **2003**, *157*, 237−245.
(57) Dillon, T. J.; Holscher, D.; Sivakumaran, V.; Horowitz, A.; Crowley, J. N. Kinetics of the Reactions of HO With Methanol (210−351 K) and With Ethanol (216−368 K). *Phys. Chem. Chem. Phys.* **2005**, *7*, 349−355.
(58) Spray, R. L.; McDonald, K. J.; Choi, K.-S. Enhancing Photoresponse of Nanoparticulate α-Fe_2O_3 Electrodes by Surface Composition Tuning. *J. Phys. Chem. C* **2011**, *115*, 3497−3506.
(59) Jo, W. J.; Jang, J.-W.; Kong, K.-J.; Kang, H. J.; Kim, J. Y.; Jun, H.; Parmar, K. P. S.; Lee, J. S. Phosphate Doping Into Monoclinic $BiVO_4$ for Enhanced Photoelectrochemical Water Oxidation Activity. *Angew. Chem., Int. Ed.* **2012**, *51*, 3147−3151.
(60) Hong, S. J.; Lee, S.; Jang, J. S.; Lee, J. S. Heterojunction $BiVO_4$/WO_3 Electrodes for Enhanced Photoactivity of Water Oxidation. *Energy Environ. Sci.* **2011**, *4*, 1781−1787.
(61) Su, J.; Guo, L.; Bao, N.; Grimes, C. A. Nanostructured WO_3/$BiVO_4$ Heterojunction Films for Efficient Photoelectrochemical Water Splitting. *Nano Lett.* **2011**, *11*, 1928−1933.
(62) Saito, R.; Maiseki, Y.; Sayama, K. Highly Efficient Photoelectrochemical Water Splitting Using a Thin Film Photoanode of $BiVO_4$/SnO_2/WO_3 Multi-composite in a Carbonate Electrolyte. *Chem. Commun.* **2012**, *48*, 3833−3835.
(63) Liang, Y.; Tsubota, T.; Mooij, L. P. A.; Van de Krol, R. Highly Improved Quantum Efficiencies for Thin Film $BiVO_4$ Photoanodes. *J. Phys. Chem. C* **2011**, *115*, 17594−17598.
(64) Leng, W. H.; Barnes, P. R. F.; Juozapavicius, M.; O'Regan, B. C.; Durrant, J. R. Electron Diffusion Length in Mesoporous Nanocrystalline TiO_2 Photoelectrodes During Water Oxidation. *J. Phys. Chem. Lett.* **2010**, *1*, 967−972.
(65) Rao, A. R.; Dutta, V. Achievement of 4.7% Conversion Efficiency in ZnO Dye-sensitized Solar Cells Fabricated by Spray Deposition Using Hydrothermally Synthesized Nanoparticles. *Nanotechnology* **2008**, *19*, 445712.